Title

Age-dependent hepatic lymphoid organization directs successful immunity to hepatitis B

Journal

Journal of Clinical Investigation, 123(9)

ISSN

0021-9738

Authors

Publicover, Jean

Gaggar, Anuj

Nishimura, Stephen

et al.

Publication Date

2013-09-03

DOI

10.1172/jci68182

Peer reviewed

Age-dependent hepatic lymphoid organization directs successful immunity to hepatitis B

Jean Publicover,[1,2] Anuj Gaggar,[1,2] Stephen Nishimura,[3] Christine M. Van Horn,[1,2] Amanda Goodsell,[1,2] Marcus O. Muench,[2,4] R. Lee Reinhardt,[5] Nico van Rooijen,[6] Adil E. Wakil,[7,8] Marion Peters,[1,2] Jason G. Cyster,[5] David J. Erle,[1] Philip Rosenthal,[2,9,10] Stewart Cooper,[2,7,8] and Jody L. Baron[1,2]

[1]Department of Medicine, [2]UCSF Liver Center, and [3]Department of Pathology, UCSF, San Francisco, California, USA. [4]Laboratory Medicine, Blood Systems Research Institute, San Francisco, California, USA. [5]Department of Microbiology and Immunology, Howard Hughes Medical Institute, UCSF, San Francisco, California, USA. [6]Vrije Universiteit Medisch Centrum, Department of Molecular Cell Biology, Faculty of Medicine, Amsterdam, The Netherlands. [7]Liver Immunology Laboratory and [8]Division of Hepatology, California Pacific Medical Center and Research Institute, San Francisco, California, USA. [9]Department of Pediatrics and [10]Department of Surgery, UCSF, San Francisco, California, USA.

Hepatitis B virus (HBV) is a major human pathogen that causes immune-mediated hepatitis. Successful immunity to HBV is age dependent: viral clearance occurs in most adults, whereas neonates and young children usually develop chronic infection. Using a mouse model of HBV infection, we sought mechanisms underpinning the age-dependent outcome of HBV and demonstrated that hepatic macrophages facilitate lymphoid organization and immune priming within the adult liver and promote successful immunity. In contrast, lymphoid organization and immune priming was greatly diminished in the livers of young mice, and of macrophage-depleted adult mice, leading to abrogated HBV immunity. Furthermore, we found that CXCL13, which is involved in B lymphocyte trafficking and lymphoid architecture and development, is expressed in an age-dependent manner in both adult mouse and human hepatic macrophages and plays an integral role in facilitating an effective immune response against HBV. Taken together, these results identify some of the immunological mechanisms necessary for effective control of HBV.

Introduction

HBV is a noncytopathic hepadnavirus that chronically infects approximately 400 million people and results in approximately 1 million deaths annually by causing liver failure and liver cancer (1). The chance of clearing acute HBV infection (a-HBV) is age dependent. 95% of adult-acquired infections lead to spontaneous clearance, whereas more than 90% of exposed neonates and approximately 30% of children aged 1–5 years fail to resolve a-HBV and develop chronic infection (2–4). Individuals infected during infancy represent the group that harbors the majority of the global reservoir of HBV and exert the greatest healthcare impact. A strong, diverse, adaptive immune response is considered essential for HBV clearance, but the mechanisms by which an individual orchestrates a favorable response are just beginning to be understood (5–8).

Unraveling the basis of failed immunity in infants and children remains experimentally challenging, owing to the intrinsic limitations of tissue acquisition from children and the fact that at-risk infants in developed countries receive immune globulin and vaccination to prevent infection. Development of robust, accessible animal models that allow mechanistic understanding of HBV disease pathogenesis has also been challenging because infection of hepatocytes with HBV is restricted to humans, and there are no known hepatotropic viruses that infect mice. To overcome this challenge, and to begin to explore the immune mechanisms that underlie the age-dependent divergent disease outcomes during a-HBV, our laboratory has developed transgenic mouse models that faithfully mimic key aspects of age-dependent immunological differences in human HBV clearance and persistence (9). We use HBV transgenic mice (2 distinct transgenes and lineages) crossed with mice genetically deficient in the recombinase *Rag1*, which is required to generate mature B and T cells (10). This produces mice that express viral antigens or intact virus in the liver in the absence of an adaptive immune system. Adoptive transfer of 10^8 HBV-naive, syngeneic splenocytes from WT C57BL/6 or genetically modified mice reconstitutes the immune system, mimics key features of primary HBV infection, and allows us to test the importance of cellular and soluble mediators in HBV pathogenesis (11). In this model, adoptive transfer of adult splenocytes into adult HBV transgenic mice crossed with *Rag1*$^{-/-}$ mice (referred to herein as HBVtg*Rag1*$^{-/-}$ mice) leads to an effective immune response and disease kinetics comparable to those seen in adult humans experiencing self-limited a-HBV. Specifically, these reconstituted adult mice generate an immune response with a strong and diverse HBV-specific T cell response and serological profile that precisely mirrors immune responses seen in the peripheral blood of patients who clear HBV infection: positive for HBV core antibody (HBcAb$^+$) and HBV surface antibody (HBsAb$^+$) and negative for HBV surface antigen (HBsAg$^-$). On the other hand, adoptive transfer of adult splenocytes into young HBVtg*Rag1*$^{-/-}$ mice leads to an immune response and disease kinetics strikingly similar to those seen in young humans who develop persistent HBV infection. Specifically, reconstituted young mice generate an immune response with a weak and narrow HBV-specific T cell response and a HBcAb$^+$HBsAb$^-$HBsAg$^+$ serological profile, which mirrors that seen in the peripheral blood of patients who develop chronic HBV infection (9). Analysis of young and adult HBVtgRag mice has revealed minimal differences in antigen expression in the plasma

Conflict of interest: The authors have declared that no conflict of interest exists.

Note regarding evaluation of this manuscript: Manuscripts authored by scientists associated with Duke University, The University of North Carolina at Chapel Hill, Duke-NUS, and the Sanford-Burnham Medical Research Institute are handled not by members of the editorial board but rather by the science editors, who consult with selected external editors and reviewers.

Citation for this article: *J Clin Invest.* 2013;123(9):3728–3739. doi:10.1172/JCI68182.

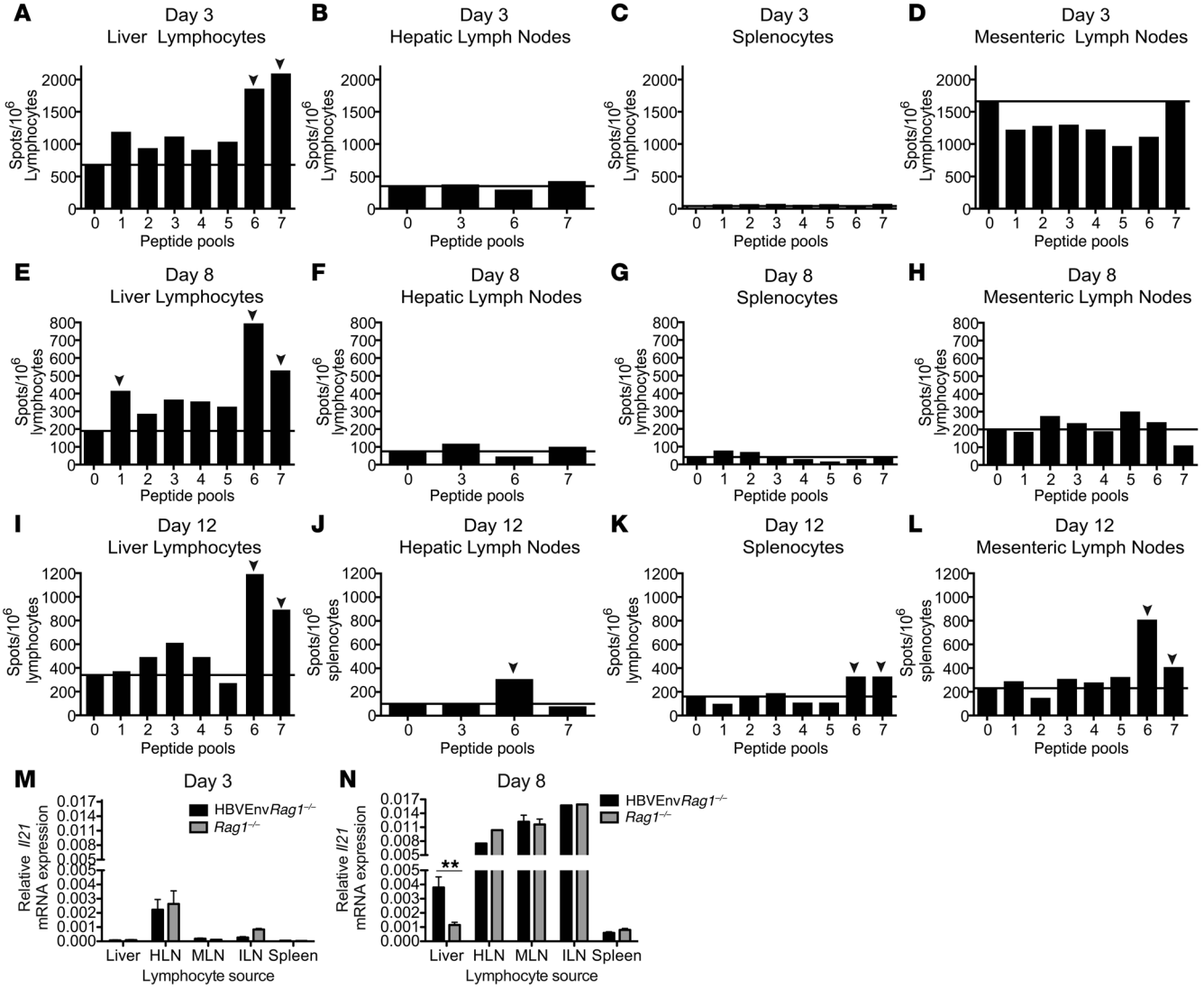

Figure 1

HBV-specific immune responses that direct viral clearance are first detected in the liver. (**A**–**L**) HBV-specific T cell responses from lymphocytes isolated from the liver (**A**, **E**, and **I**), HLNs (**B**, **F**, and **J**), spleen (**C**, **G**, and **K**), and MLNs (**D**, **H**, and **L**) at days 3 (**A**–**D**), 8 (**E**–**H**), and 12 (**I**–**L**) after adoptive transfer of adult WT syngeneic splenocytes into adult HBVEnv*Rag1*$^{-/-}$ mice. Lymphocytes were stimulated with pools of HBV-envelope–derived peptides (15-mer peptides; pools of 12–14). IFN-γ was measured by ELISpot assay; representative data from 2 separate experiments are shown. Samples were pooled from $n \geq 3$ mice. Pool 0 denotes no peptide; solid lines denote baseline IFN-γ levels; arrowheads denote a positive response ≥2× that of baseline. (**M** and **N**) *Il21* mRNA expression levels from lymphocytes isolated from adult HBVEnv*Rag1*$^{-/-}$ and *Rag1*$^{-/-}$ liver, spleen, MLNs, HLNs, and ILNs at 3 (**M**) and 8 (**N**) days after adoptive transfer of WT syngeneic splenocytes. *Il21* levels relative to *Gapdh* were determined by real-time PCR. Data are representative of at least 2 independent experiments. $^{**}P = 0.0048$, unpaired 2-tailed Student's *t* test.

or liver (9, 11). Both age groups demonstrate overlapping plasma levels and hepatocyte expression of HBsAg as well as plasma viral load, demonstrating that the observed age-related differences in immune response in our model likely do not result from differences in antigen expression.

Using this age-dependent model, we have made progress in elucidating potential mechanisms by which the immaturity of the immune-priming environment of effector lymphocytes in newborns and young children contributes significantly to the attenuated immune response that leads to HBV persistence and chronic hepatitis. Specifically, we have previously shown that IL-21 production in the adult liver by T follicular helper (TFH) cells facilitates an effective immune response to HBV and that TFH cell number and IL-21 production is greatly diminished in the livers of young mice that mount an ineffective immune response to HBV. Furthermore, the finding that TFH IL-21 production and the HBV-specific adaptive immune response are liver centered invokes the hypothesis that physiologically important hepatic immune priming may be required for natural HBV immunity.

To explore this hypothesis, and to dissect the cellular and molecular pathways underlying age-dependent differences in immune priming, we used liver-specific immune assays coupled with immunofluorescent staining of liver sections and genome-wide microarray analysis to compare livers from young and adult HBVtg*Rag1*$^{-/-}$ mice. Here,

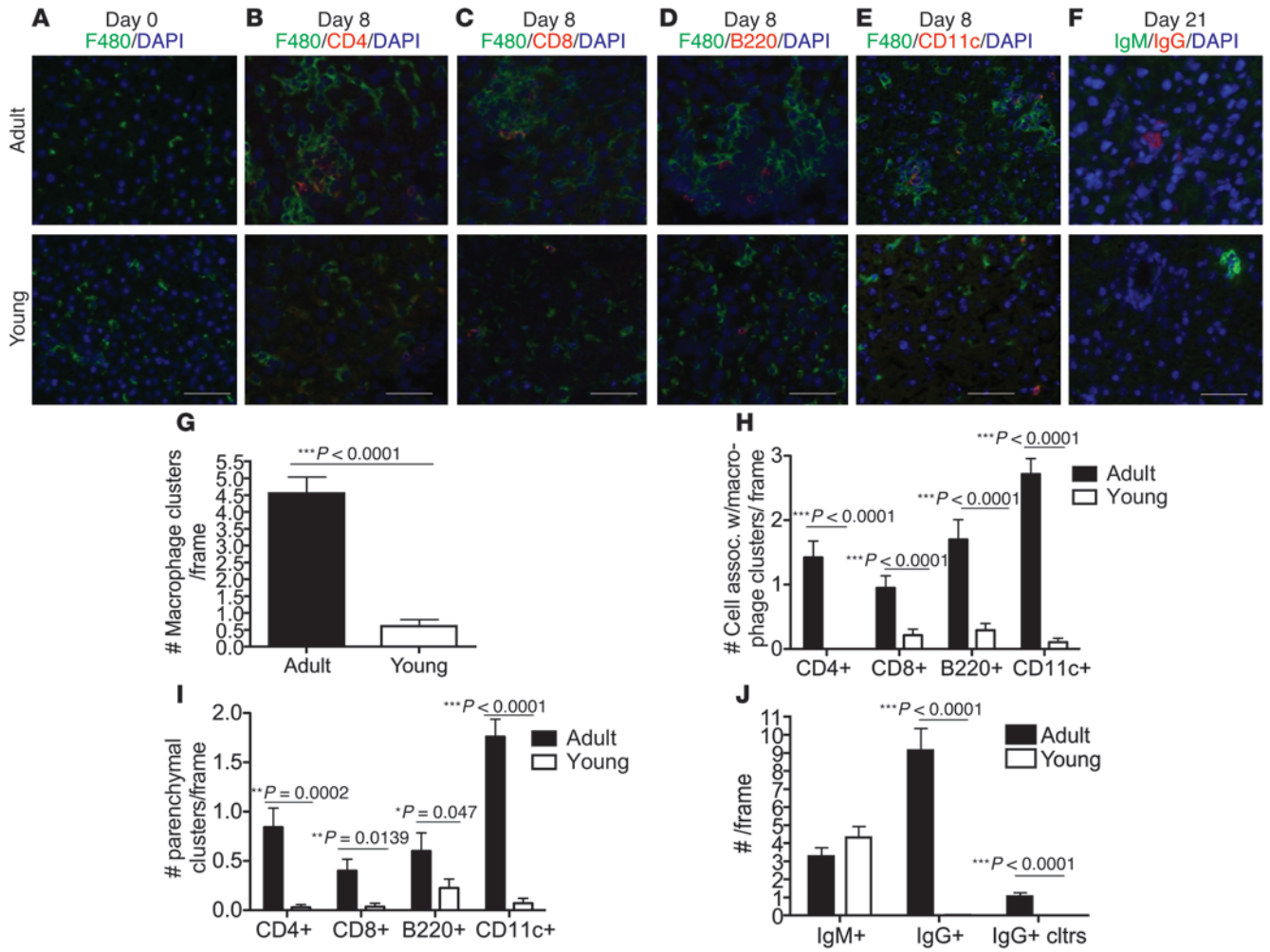

Figure 2

Adult mice show increased macrophage-associated lymphocyte organization, parenchymal lymphocyte clustering and IgG$^+$ B cells compared to young mice. (**A**) Representative images (original magnification, ×10) of macrophage (green; F4/80) and nuclei (DAPI; blue) staining of adult (top) and young (bottom) HBVEnv*Rag1*$^{-/-}$ mouse liver tissue prior to adoptive transfer. (**B**–**E**) Representative images (original magnification, ×10) of F4/80 (green), DAPI (blue), and CD4 (red; **B**), CD8 (red; **C**), B cells (red; B220; **D**) or DCs (red; CD11c; **E**) staining of adult and young HBVEnv*Rag1*$^{-/-}$ liver tissue 8 days after adoptive transfer of adult WT splenocytes. Livers were frozen in OCT, sectioned at 6-μm thickness, and acetone fixed. (**G**–**I**) 15 random frames per section of $n \geq 3$ mice per group were scored by an unbiased pathologist for (**G**) number of macrophage clusters, defined as ≥4 macrophages adjacent to each other/frame; (**H**) number of CD4$^+$, CD8$^+$, B220$^+$, or CD11c$^+$ cells interacting with macrophage cluster/frame; and (**I**) number of parenchymal CD4$^+$, CD8$^+$, B220$^+$ lymphocyte clusters/frame (≥2 cells within 15 μm). (**F**) Representative images (original magnification, ×10) of IgM (green), IgG (red; pooled IgG1 and IgG2b), and DAPI (blue) staining of adult and young liver tissue 21 days after adoptive transfer. (**J**) 15 random frames per section of $n \geq 3$ mice per group were scored by an unbiased pathologist for number of IgM$^+$ cells, IgG$^+$ cells, and IgG clusters per frame (≥2 cells within 15 μm). Scale bars: 30 μm. $^*P < 0.05$, $^{**}P < 0.01$, $^{***}P < 0.001$, unpaired 2-tailed Student's *t* test.

we found that age-dependent development of hepatic macrophages facilitated lymphoid organization and immune priming within the adult liver, and this lymphoid organization and immune priming was greatly diminished in the livers of young mice or of adult mice depleted of macrophages. In addition, our data indicated that age-dependent expression of CXCL13 by adult hepatic macrophages contributes to liver lymphoid organization in mice and humans and facilitates effective immune responses to HBV.

Results

HBV-specific T cell responses and HBV-dependent IL-21 expression are first detected in the liver, followed by detection in LNs and spleen. Previous studies using our mouse model demonstrated that HBV-specific immune responses are found in the liver, but not in the spleen, at 8 days, 3 months, and 1 year after adoptive transfer of splenocytes (9). To identify the site of immune priming and the anatomical locations of the immune response, we examined HBV-specific T cell responses during the first 12 days after adoptive transfer of 10^8 adult syngeneic splenocytes into adult HBV transgenic mice expressing the small, middle, and large envelope proteins of HBV crossed with *Rag1*$^{-/-}$ mice (referred to herein as HBVEnv*Rag1*$^{-/-}$ mice). The following sites were sampled: mesenteric LNs (MLNs; located between the gut and the liver), liver parenchyma, hepatic LNs (HLNs; which drain the liver) (12), and spleen. To detect HBV-specific T cell responses from the various sites, we stimulated lymphoid cells with pools of peptides spanning the entire HBV envelope proteins and assayed

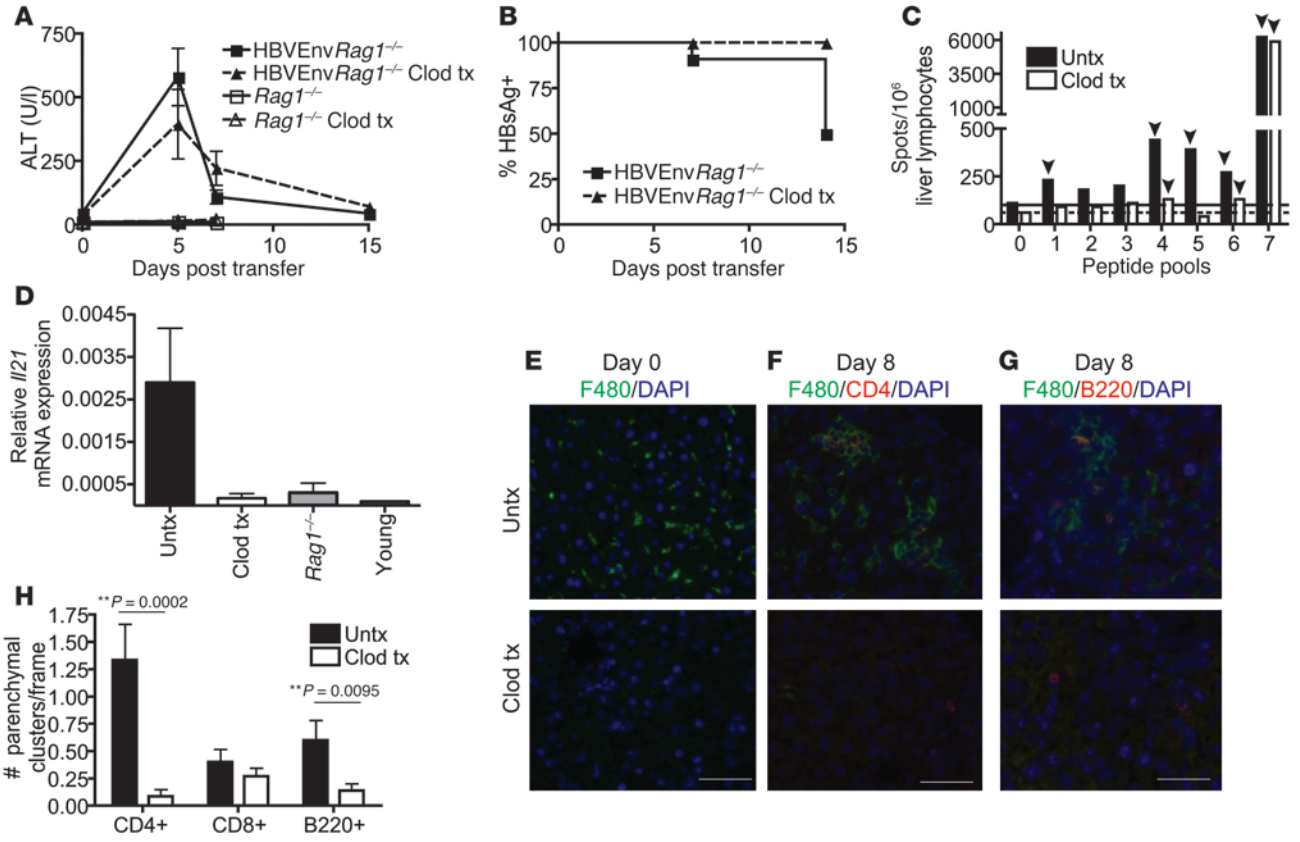

Figure 3

Macrophage depletion leads to an immune response that correlates with chronic HBV and impaired hepatic lymphocyte organization. (**A** and **B**) HBVEnv*Rag1*$^{-/-}$ mice were treated (tx) or not (untx) with clodronate liposome (Clod) on days –1, 2, 5, 8, and 11 and adoptively transferred on day 0 with WT splenocytes ($n \geq 5$). (**A**) Plasma ALT. (**B**) Percent mice with circulating HBsAg. (**C**) HBV-specific T cell responses, identified by IFN-γ ELISpot, using liver-derived lymphocytes from clodronate-treated or untreated HBVEnv*Rag1*$^{-/-}$ mice 4 months after transfer. Data are pooled from $n \geq 4$ mice. Pool 0 denotes no peptide; solid and dotted lines denote baseline IFN-γ levels for untreated and clodronate-treated, respectively; arrowheads denote a positive response ≥2× that of baseline. (**D**) *Il21* mRNA expression levels in liver-derived lymphocytes from untreated and clodronate-treated adult HBVEnv*Rag1*$^{-/-}$ mice, untreated adult *Rag1*$^{-/-}$ mice, and untreated young HBVEnv*Rag1*$^{-/-}$ mice 8 days after transfer, determined by RT-PCR ($n \geq 2$). Data are representative of 3 (**A**, **B**, and **D**) or 2 (**C**) independent experiments. (**E**–**G**) Images (original magnification, ×10) from untreated and clodronate-treated HBVEnv*Rag1*$^{-/-}$ liver stained for (**E**) macrophages (green; F4/80) and nuclei (blue; DAPI) before adoptive transfer (day 0) or for F4/80 (green), DAPI (blue), and either CD4 (red; **F**) or B220 (red; **G**) 8 days after transfer. (**H**) 15 random frames from each section of $n \geq 3$ mice per group were scored by an unbiased pathologist for number of parenchymal CD4$^+$, CD8$^+$, and B220$^+$ lymphocyte clusters per frame (≥2 cells within 15 μm). Scale bars: 30 μm. $^{**}P < 0.01$, unpaired 2-tailed Student's *t* test.

for HBV-specific IFN-γ production using ELISpot assays (9). These ELISpot assays demonstrated that liver parenchyma–derived T cells mounted an IFN-γ response to multiple HBV envelope peptides 3 days after adoptive transfer, with a more robust response present after 8 and 12 days (Figure 1, A, E, and I). In contrast, we failed to detect HBV-specific responses in the spleen, MLN, or HLN at 1, 2, 3, or 8 days after adoptive transfer and only began to detect HBV-specific responses at these sites after 12 days (Figure 1, B–D, F–H, and J–L, and data not shown). The lack of HBV-specific T cells responses at various immune sites did not reflect a paucity of lymphocytes or a lack of antigen expression, since we could easily detect HBsAg and repopulation with B and T cells 3 and 8 days after adoptive transfer at these sites (Supplemental Figure 1; supplemental material available online with this article; doi:10.1172/JCI68182DS1).

To confirm these results and validate our ELISpot assay, we also studied HBV-specific T cell responses at the various sites using the same peptide pools, but using an IFN-γ cytokine capture assay. This assay corroborates our ELISpot assay results that we could not detect HBV-specific T cells in the spleen or LNs 3 days after adoptive transfer, and further suggests that HBV-specific CD4$^+$ T cells may begin to populate the HLNs that drain the liver on day 8 after adoptive transfer. Furthermore, the assay demonstrated that both CD4$^+$ and CD8$^+$ T cells contributed to the antiviral response (Supplemental Figure 2 and data not shown).

Our previous studies demonstrated increased, HBV-specific *Il21* mRNA expression and IL-21 cytokine secretion from TFH cells in the livers of adult mice 8 days after adoptive transfer of adult splenocytes compared with young mice as well as a critical role for IL-21 in a-HBV outcome (9). To determine the timing and site of this HBV-specific IL-21 expression, we analyzed the relative expression of *Il21* mRNA from the lymphoid cells derived from the MLN, HLN, liver parenchyma, and spleen as well as the anatomically distant inguinal LNs (ILNs) of adult HBVEnv*Rag1*$^{-/-}$ and *Rag1*$^{-/-}$ mice 3, 5, and 8 days after adoptive transfer. We observed no evidence of

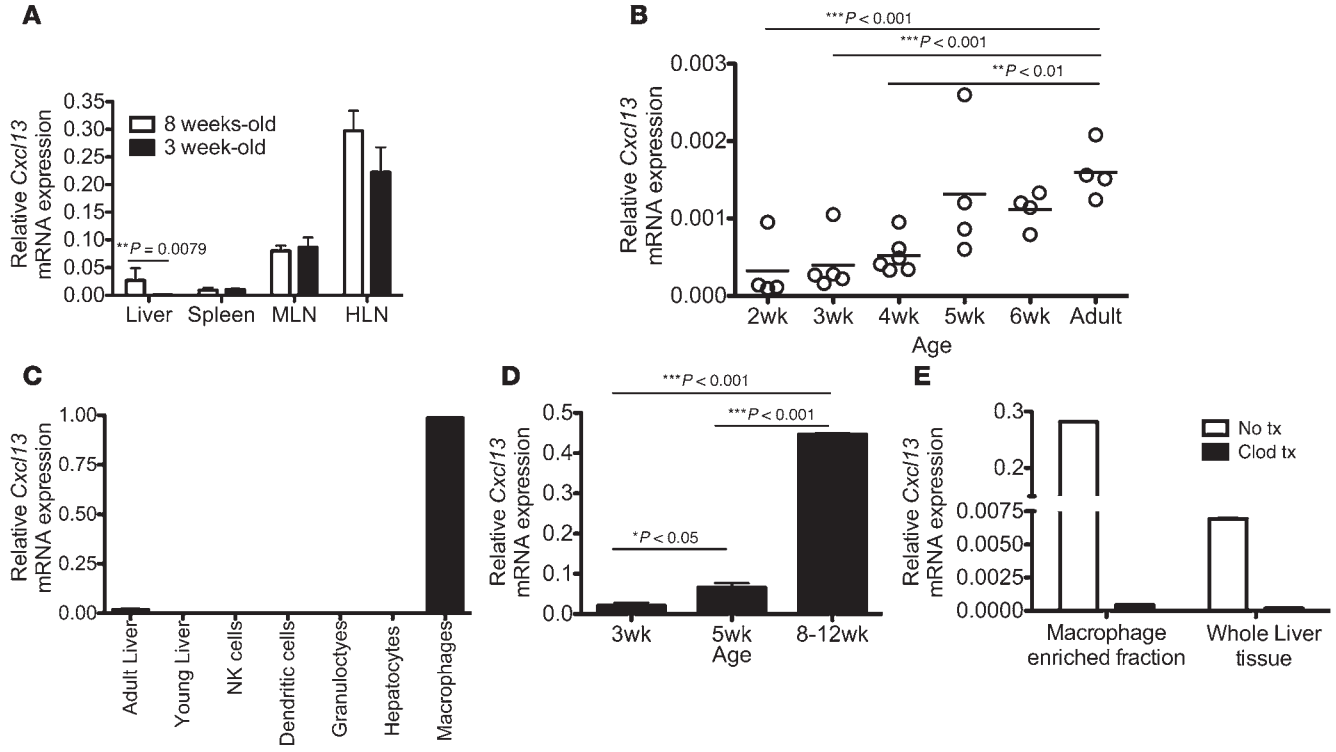

Figure 4

Age-dependent hepatic CXCL13 expression is by macrophages and is susceptible to clodronate liposome treatment. (**A**) *Cxcl13* mRNA expression relative to *Gapdh* in 3- and 8-week-old *Rag1*$^{-/-}$ mouse liver, spleen, MLNs, and HLNs. ($n \geq 4$). Data are representative of 2 independent experiments. (**B**) Relative *Cxcl13* mRNA expression from liver of WT mice at the indicated ages. Data are representative of 2 independent experiments. (**C**) *Cxcl13* mRNA expression levels in whole liver of adult and young *Rag1*$^{-/-}$ mice and in sorted cell populations from adult *Rag1*$^{-/-}$ liver. Cells were isolated using liver perfusion with DNAse and collagenase, followed by gradient separation and sorting for viability and the following parameters: NK cells (NK1.1$^+$), DCs (NK1.1$^-$CD11c$^+$CD11b$^-$), granulocytes/monocytes (NK1.1$^-$CD11b$^+$F4/80$^-$). Macrophages were enriched by liver perfusion with DNase and collagenase followed by 30-minute incubation with pronase, isolated using a 25:50 Percoll gradient and sorted for CD45$^+$CD11b$^+$F4/80$^+$. Hepatocytes were isolated and sorted by flow cytometry based on size and viability. (**D**) *Cxcl13* mRNA expression in unsorted macrophage-enriched fractions from liver of *Rag1*$^{-/-}$ mice aged 3, 5, and 8–12 weeks ($n = 3$). (**E**) Relative CXCL13 levels in whole liver and macrophage-enriched fractions from adult *Rag1*$^{-/-}$ mice that were untreated or treated with clodronate 48 hours earlier (data are representative of 3 independent experiments). *$P < 0.05$, **$P < 0.01$, ***$P < 0.001$, Mann-Whitney test (**A**) or Tukey's ANOVA multiple-comparison test (**B** and **D**).

HBV-specific *Il21* expression 3 and 5 days after adoptive transfer (Figure 1M and data not shown). At 8 days after adoptive transfer, we observed HBV-independent increases in *Il21* mRNA expression in all LNs and spleens of both *Rag1*$^{-/-}$ and HBVEnv*Rag1*$^{-/-}$ mice (Figure 1N), suggesting a de novo population of these lymphoid organs with adoptively transferred lymphocytes. However, significant HBV-specific *Il21* expression at day 8 was only observed in the liver. Taken together, our previous studies (9) and the present findings further support our hypothesis that immune priming and differentiation occurs within the liver; moreover, this immune priming and differentiation is not as effective in the young liver.

Adult mice develop hepatic clusters of macrophages, DCs, B cells, and T cells during the acute immune response to HBV that are significantly diminished in young liver. To seek evidence for hepatic lymphoid organization and immune priming during a-HBV, we used immunofluorescent staining of liver sections from young and adult HBVEnv*Rag1*$^{-/-}$ mice before and after adoptive transfer of syngeneic adult splenocytes. Before adoptive transfer of splenocytes, the both young and adult HBVEnv*Rag1*$^{-/-}$ livers had similar numbers of F4/80$^+$ macrophages that were uniformly distributed as single cells throughout the liver (Figure 2A). However, 8 days after adoptive transfer, adult livers had extensive intraparenchymal clusters of macrophages, which coclustered with CD4$^+$ T cells, CD8$^+$ T cells, B cells, and highly arborized CD11c$^+$ cells morphologically consistent with DCs (Figure 2, B–E, G, and H). These intraparenchymal clusters were located between the portal triads and central veins and never merged with portal triads; thus, they were not extensions of portal-based inflammation. Macrophage clustering and colocalization with T and B cells and DCs were significantly diminished in young livers (Figure 2, B–E, G, and H). Furthermore, adult livers displayed intraparenchymal clusters of CD4$^+$ T cells, CD8$^+$ T cells, B cells, and DCs that was significantly reduced in young livers (Figure 2, B–E and I). Finally, consistent with our previous finding of diminished class-switched B cells in young livers (9), we observed equivalent numbers of IgM$^+$ cells in young and adult liver parenchyma, but significantly diminished numbers of IgG$^+$ cells and IgG$^+$ clusters in young livers, 21 days after adoptive transfer (Figure 2, F and J).

Hepatic macrophages in adult mice facilitate lymphoid organization and an effective immune response to HBV. Because F4/80$^+$ macrophages appear to anchor the lymphoid organization within the adult liver, we tested the hypothesis that depletion of these cells

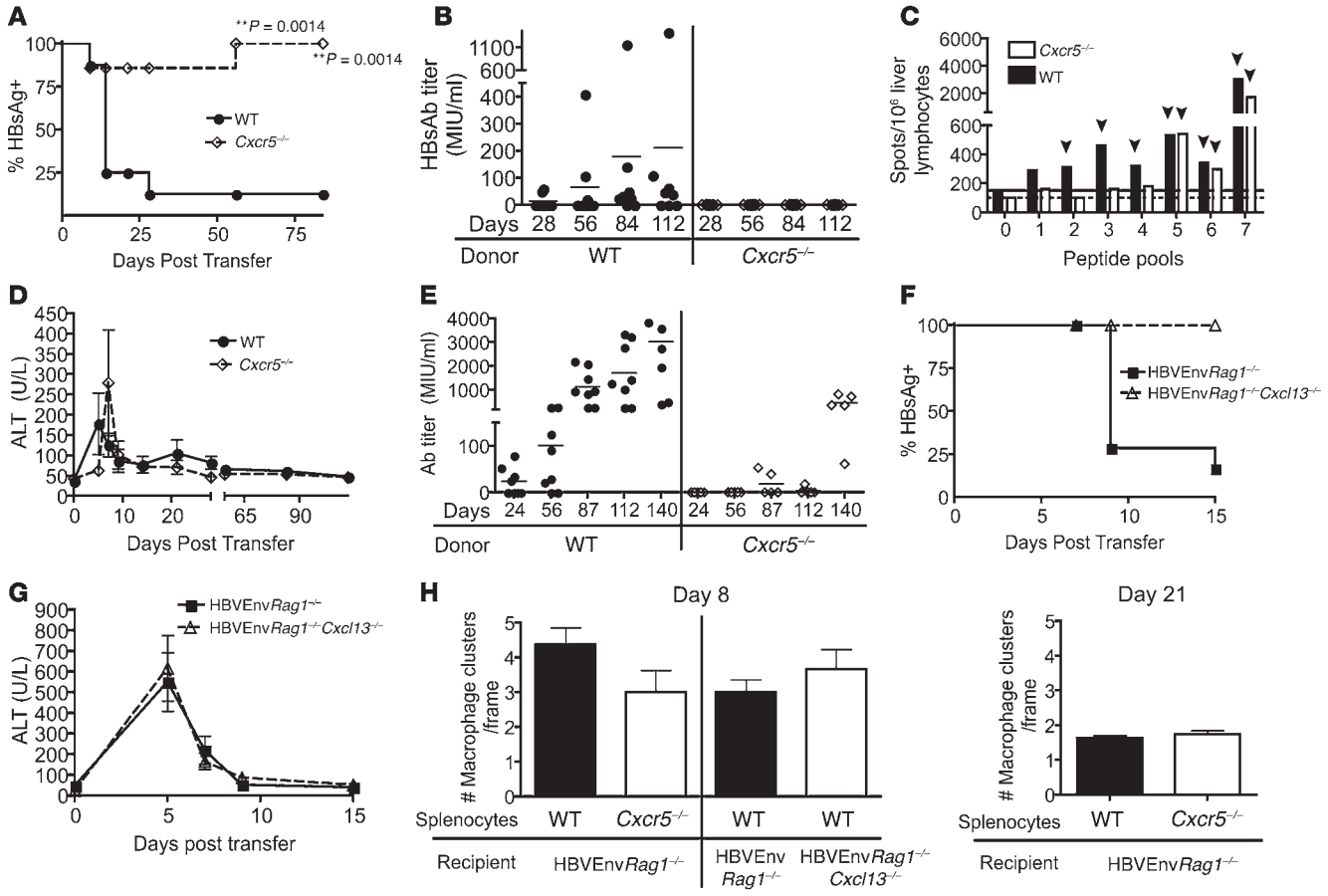

Figure 5

Absence of CXCR5 on donor splenocytes or CXCL13 in recipient mice impairs the adaptive immune response to HBV. (**A**) Percentage of mice with circulating HBsAg and (**B**) plasma HBsAb titer in HBVEnv*Rag1*$^{-/-}$ recipients of WT or *Cxcr5*$^{-/-}$ adult splenocytes. (**C**) HBV-specific T cell responses 4 months after transfer, identified by IFN-γ ELISpot, using liver-derived lymphocytes from HBVEnv*Rag1*$^{-/-}$ recipients of WT or *Cxcr5*$^{-/-}$ splenocytes. Data are pooled from $n = 4$ mice. Pool 0 denotes no peptide; solid and dotted lines denote baseline IFN-γ levels for WT and *Cxcr5*$^{-/-}$ recipient mice, respectively; arrowheads denote a positive response ≥2× that of baseline. (**D**) Plasma ALT levels in HBVEnv*Rag1*$^{-/-}$ mice adoptively transferred with WT or *Cxcr5*$^{-/-}$ splenocytes. (**E**) HBsAb response in WT and *Cxcr5*$^{-/-}$ mice vaccinated with HBV vaccine (Merck) intramuscularly at days 0 and 56. (**F**) Percentage of mice with circulating HBsAg and (**G**) plasma ALT levels in HBVEnv*Rag1*$^{-/-}$ or HBVEnv*Rag1*$^{-/-}$*Cxcl13*$^{-/-}$ mice adoptively transferred with WT splenocytes. Data are representative of 3 (**A**, **B**, and **D**) or 2 (**C** and **E**–**G**) independent experiments. (**H**) Macrophage clustering in HBVEnv*Rag1*$^{-/-}$ mouse liver tissue 8 and 21 days after adoptive transfer of WT or *Cxcr5*$^{-/-}$ splenocytes and in HBVEnv*Rag1*$^{-/-}$ or HBVEnv*Rag1*$^{-/-}$*Cxcl13*$^{-/-}$ mouse liver tissue 8 days after adoptive transfer of WT splenocytes. $^{**}P = 0.0014$, Fisher's χ^2 test.

before adoptive transfer would alter the lymphoid organization and subsequent immune response to HBV in the adult mice. To deplete macrophages, adult HBVEnv*Rag1*$^{-/-}$ mice were treated with 5 doses of clodronate liposomes (13) every 3 days, beginning 1 day before adoptive transfer of adult splenocytes. This treatment led to hepatic depletion of F4/80$^+$ cells for 15 days (Figure 3E and data not shown). Adult HBVEnv*Rag1*$^{-/-}$ mice that received clodronate treatment still developed the HBV-dependent hepatitis observed in untreated mice, as evidenced by an increase in plasma alanine transaminase (ALT; Figure 3A). However, similar to the young mice, they failed to clear HBsAg from blood and did not develop the robust and epitopically diverse HBV-specific memory T cell response typically seen in adult mice (Figure 3, B and C). Furthermore, in adult mice that received clodronate treatment, HBV-specific *Il21* mRNA levels in liver lymphoid cells were diminished, to levels similar to those observed in young mice (Figure 3D).

Immunofluorescent staining of livers revealed that clodronate depletion also significantly altered the lymphoid organization observed in HBVEnv*Rag1*$^{-/-}$ adult liver 8 days after adoptive transfer. Specifically, the number of parenchymal CD4$^+$ T cell clusters and B220$^+$ B cell clusters were significantly diminished in clodronate-treated mice (Figure 3, F–H), which suggests that lymphocyte clustering observed in the adult mice is dependent on hepatic macrophages. Interestingly, the number of CD8$^+$ T cell clusters was not affected by macrophage depletion.

Age-dependent expression of the chemokine CXCL13 is observed exclusively in the liver, and CXCL13 is predominantly produced by hepatic macrophages. In order to identify differences in the liver immune priming environment of adult and young mice, we used genome-wide microarray analysis to compare livers from young and adult HBVEnv*Rag1*$^{-/-}$ mice before adoptive transfer of a naive immune system. Data from microarray analysis, verified by real-time PCR, demonstrated a 9-fold increase in mRNA expression of the che-

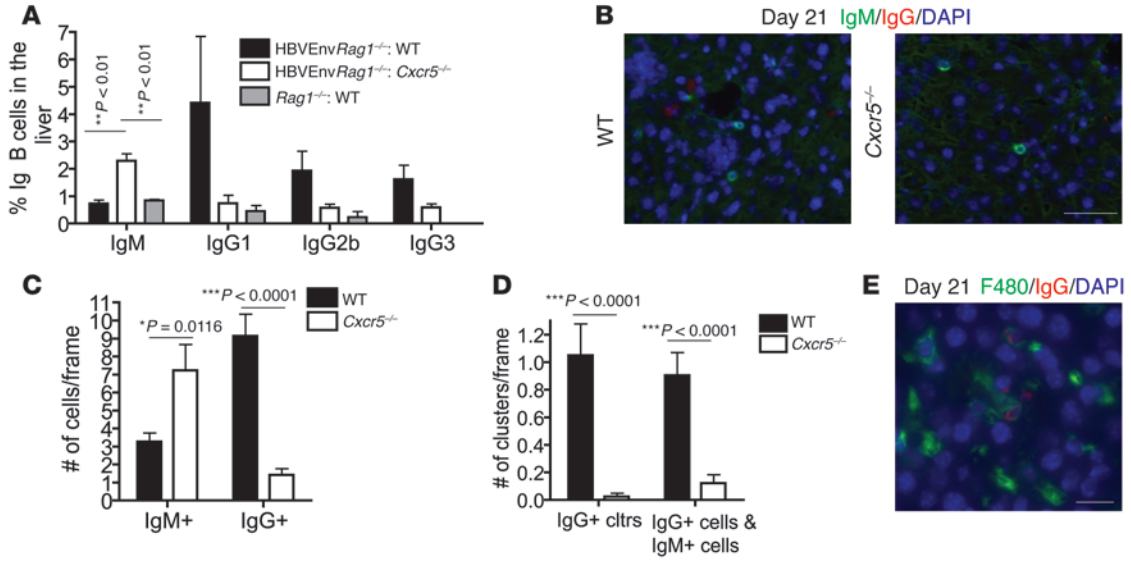

Figure 6

Absence of CXCR5 on donor splenocytes alters hepatic IgM$^+$ and IgG$^+$ B cell number and B cell clustering. (**A**) Frequency of B cells (plasma cells and plasmablasts) determined by FACS analysis on liver lymphocytes isolated 3 weeks after transfer of HBVEnv*Rag1*$^{-/-}$ or *Rag1*$^{-/-}$ mice with WT or *Cxcr5*$^{-/-}$ splenocytes. Percentage of IgG1, IgG2b, and IgG3 B cell (B220^{lo}TCR-β$^-$CD44^{hi}) and IgM B cell (B220^{lo}TCR-β$^-$) populations were identified in liver-derived lymphocytes by FACS (n = 3). (**B**) Representative images (original magnification, ×10) from liver tissue of HBVEnv*Rag1*$^{-/-}$ mice 21 days after adoptive transfer of WT or *Cxcr5*$^{-/-}$ splenocytes, stained for IgM (green), IgG (red; IgG1 and IgG2b pooled) and DAPI (blue). (**C** and **D**) 15 random frames per section of $n \geq 3$ mice per group were blinded and analyzed for (**C**) number of IgM$^+$ and IgG$^+$ cells and (**D**) number of IgG lymphocyte clusters (≥2 cells within 15 μm) and IgG$^+$ cells associated with ≥1 IgM$^+$ cell per frame. (**E**) Representative image (original magnification, ×40) from HBVEnv*Rag1*$^{-/-}$ mouse liver stained for F4/80 (green), IgG (red; IgG1 and IgG2b pooled), and DAPI (blue) 21 days after adoptive transfer of WT syngeneic splenocytes. Scale bars: 30 μm (**B**); 10 μm (**E**). $^*P < 0.05$, $^{**}P < 0.01$, $^{***}P < 0.001$, Tukey's ANOVA multiple-comparison test (**A**) or unpaired 2-tailed Student's t test (**C** and **D**).

mokine ligand *Cxcl13* in the livers of adult (8–10 weeks old) versus young (3 weeks old) HBVEnv*Rag1*$^{-/-}$ mice (data not shown). This age-dependent *Cxcl13* expression was not dependent on HBV antigen expression, nor was it particular to *Rag1*$^{-/-}$ mice, because we also observed age-dependent expression in the livers of young and adult *Rag1*$^{-/-}$ and WT C57BL/6 mice (Figure 4, A and B). This age-dependent difference in expression was not observed in the spleen or LNs; both young and adult mice had ample *Cxcl13* expression in these lymphoid organs (Figure 4A). Thus, age-dependent differences in CXCL13 expression appear to be unique to the liver. Strikingly, expression of *Cxcl13* in the liver begins to increase to adult levels by 5 weeks of age (Figure 4B), the same time at which the immune response to HBV in our model begins to convert to the adult response. Inflammation in the liver 8 days after adoptive transfer of splenocytes did not alter hepatic expression levels of *Cxcl13* in young and adult mice (Supplemental Figure 3F).

To determine which cells in the adult liver express CXCL13, we isolated parenchymal and nonparenchymal cells from the livers of *Rag1*$^{-/-}$ mice and purified the various cell populations using fluorescent-activated cell sorting (FACS). Relative levels of *Cxcl13* mRNA from adult and young whole *Rag1*$^{-/-}$ mouse liver compared with sorted populations from adult *Rag1*$^{-/-}$ mouse liver were determined. *Cxcl13* expression in the liver was predominantly in liver macrophages (CD45$^+$CD11b$^+$F4/80$^+$) and was not detected in liver-derived NK cells, DCs, granulocytes, or hepatocytes (Figure 4C). Similarly, *Cxcl13* was not expressed by liver sinusoidal endothelial cells or hepatic stellate cells (Supplemental Figure 3, A–E). In addition, expression of *Cxcl13* in macrophage-enriched fractions was significantly age dependent (Figure 4D).

To further demonstrate that hepatic expression of CXCL13 is exclusively on nonparenchymal cells, and largely on liver macrophages, we depleted macrophages using intravenously administered clodronate liposomes (13). Immunofluorescent staining of liver sections from adult *Rag1*$^{-/-}$ mice 24 hours after clodronate injection demonstrated effective depletion of all F4/80$^+$ cells from the liver (Figure 3E). Determination of *Cxcl13* mRNA derived from clodronate-treated and untreated mice demonstrated that clodronate decreased *Cxcl13* expression in whole liver, and in the liver-derived macrophage/monocyte enriched fraction, to levels below those detected in young mice (Figure 4E and Supplemental Figure 4).

CXCL13 in recipient mice and its receptor, CXCR5, on transferred splenocytes are necessary for an effective immune response to HBV. Expression of CXCL13 (along with its receptor, CXCR5) in LNs is involved in B lymphocyte trafficking, lymphoid architecture development, and B cell Ig class switching (14–16). While CXCR5 and CXCL13 are involved in these processes, it should be noted that *Cxcr5*$^{-/-}$ mice are not globally impaired in their ability to develop antibody responses, and can still produce normal levels of switched Ig isotypes in vivo after immunization with antigen in adjuvant or in response to viral infection, and can develop functional germinal centers (16–18). This knowledge, together with our data demonstrating age-dependent expression of hepatic CXCL13, led us to test the hypothesis that CXCR5 engagement with its ligand contributes to the type of immune response that leads to HBV clearance.

We first adoptively transferred splenocytes from adult *Cxcr5*$^{-/-}$ or WT C57BL/6 (*Cxcr5*$^{+/+}$) mice into adult HBVEnv*Rag1*$^{-/-}$ mice. Flow cytometric analysis of the spleens and livers from these mice 8 days after adoptive transfer revealed that both experimental

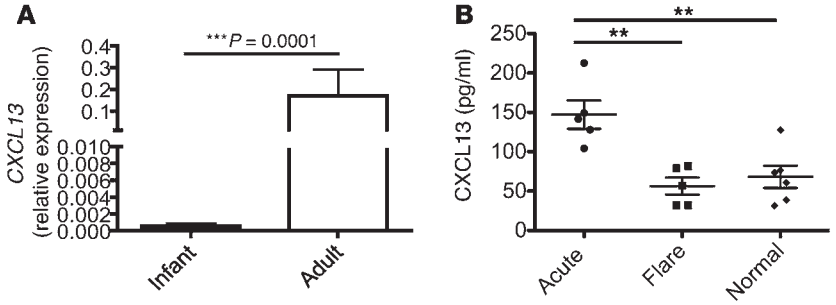

Figure 7

Adult human liver shows greater CXCL13 expression than infant liver, and plasma CXCL13 expression is significantly increased in patients who clear a-HBV. (**A**) Fresh frozen paraffin-embedded liver biopsy samples from infants 6–12 weeks of age (n = 24) and adults (n = 9) was used for RNA extraction using RNeasy FFPE kit (Qiagen), and expression of *CXCL13* relative to *GAPDH* was determined by RT-PCR. Infant liver tissue was obtained from liver biopsies performed to rule out a diagnosis of biliary atresia; of the 24 patients, 6 had biliary atresia, 6 had neonatal nonviral hepatitis, 10 had nonspecific liver disease diagnosis including cholestatsis and ductopenia, and 2 had an unknown diagnosis. Adult liver samples were obtained from donor livers prior to transplant. (**B**) Plasma was obtained from 5 patients with confirmed a-HBV infection at the time of active hepatitis and with confirmed subsequent viral clearance and HBsAb seroconversion, 5 patients with confirmed chronic HBV infection exhibiting a flare of disease, and 6 healthy volunteers and assayed for CXCL13 levels by ELISA. ***P < 0.001, Mann-Whitney test; **P = 0.0016, Tukey's ANOVA multiple-comparison test.

groups demonstrated similar homing and lymphocyte distribution in these organs (Supplemental Figure 5). However, in contrast to mice receiving WT splenocytes, *Cxcr5*$^{-/-}$ splenocyte recipients generated an ineffective immune response to HBV (Figure 5, A–C), similar to that generated in young HBVtg*Rag1*$^{-/-}$ mice (9), which fails to result in HBV immunity. Specifically, expression of CXCR5 on adoptively transferred adult splenocytes was necessary for clearance of HBsAg and for HBsAb seroconversion (Figure 5, A and B). In addition, ELISPOT analysis on liver lymphoid cells revealed that expression of CXCR5 on adoptively transferred adult splenocytes was necessary to generate an epitopically diverse HBV-specific memory T cell response (Figure 5C). Expression of CXCR5 was therefore crucial for HBV immunity.

Similar to mice that received clodronate liposomes to deplete macrophages before adoptive transfer, HBVEnv*Rag1*$^{-/-}$ mice that received *Cxcr5*$^{-/-}$ splenocytes developed acute hepatitis, as evidenced by a rise in serum ALT (Figure 3A and Figure 5D). This result intriguingly suggests that mechanisms leading to hepatocyte injury in the adult mice are different from the mechanisms responsible for HBsAb seroconversion, diversification of HBV-specific T cell responses, and clearance of HBsAg. Furthermore, similar to young mice and humans (9), adult *Cxcr5*$^{-/-}$ mice mounted a slightly dampened, but present, antibody response to HBsAg after administration of the human HBV vaccine and also generated HBcAb (Figure 5E and data not shown). This result demonstrates that *Cxcr5*$^{-/-}$ mice and young mice, like young humans, can generate a B cell response that leads to HBsAb production if the antigen is presented in the spleen and LNs, but suggests that if the antigen is presented naturally in the liver, when CXCR5 is absent, a HBsAb response cannot be generated (Figure 5, B and E).

To determine the reciprocal role of CXCL13, the ligand for CXCR5, in facilitating an effective immune response to HBV, we crossed HBVEnv*Rag1*$^{-/-}$ mice to *Cxcl13*$^{-/-}$ mice (referred to herein as HBVEnv*Rag1*$^{-/-}$*Cxcl13*$^{-/-}$ mice). Consistent with our hypothesis, adoptive transfer of WT splenocytes into adult HBVEnv*Rag1*$^{-/-}$*Cxcl13*$^{-/-}$ mice demonstrated that these animals also did not clear HBsAg from plasma (Figure 5F). Similar to adult HBVEnv*Rag1*$^{-/-}$ mice that received *Cxcr5*$^{-/-}$ splenocytes, HBVEnv*Rag1*$^{-/-}$*Cxcl13*$^{-/-}$ mice did develop HBV-dependent acute hepatitis (Figure 5G). Unfortunately, the lineage of HBVEnv*Rag1*$^{-/-}$*Cxcl13*$^{-/-}$ mice is extremely fragile, and they do not survive beyond 18 days after adoptive transfer, precluding long-term studies in this strain.

To uncover the role of CXCR5-CXCL13 interaction in the immune response to HBV, we analyzed lymphoid organization, IL-21 expression, and B cell class switching in the livers of adult HBVEnv*Rag1*$^{-/-}$ mice reconstituted with WT or *Cxcr5*$^{-/-}$ splenocytes and in HBVEnv*Rag1*$^{-/-}$*Cxcl13*$^{-/-}$ mice reconstituted with WT adult splenocytes. At 8 days after adoptive transfer, we observed similar macrophage clustering, similar B and T cell colocalization to the macrophage clusters, and similar hepatic IL-21 expression in all experimental groups (Figure 5H and Supplemental Figure 6). However, at 21 days after adoptive transfer, at the time we typically began to detect HBsAb, there was a distinct difference in the number of IgM$^+$ and IgG$^+$ B cells. We conducted flow cytometric analysis of Ig expression on plasma cells and plasmablasts derived from the livers of adult HBVEnv*Rag1*$^{-/-}$ mice that received WT or *Cxcr5*$^{-/-}$ splenocytes. *Cxcr5*$^{-/-}$ splenocyte recipients had greater numbers of plasma cells and plasmablasts expressing IgM, whereas WT splenocyte recipients had greater numbers of B cells that had differentiated into IgG1-, IgG2b-, and IgG3-expressing cells (Figure 6A). The increased presence of IgM$^+$ and IgG$^+$ plasma cells and plasmablasts in the liver was HBV specific, as we observed very few of these cells in the liver of adult *Rag1*$^{-/-}$ recipients of WT splenocytes (Figure 6A). Furthermore, immunofluorescent staining of liver sections from HBVEnv*Rag1*$^{-/-}$ recipients of WT or *Cxcr5*$^{-/-}$ splenocytes confirmed this result: 21 days after adoptive transfer, there was a significantly greater number of IgM$^+$ cells in the livers of *Cxcr5*$^{-/-}$ splenocyte recipients and a significantly greater number of IgG$^+$ cells in the livers of WT splenocyte recipients (Figure 6, B and C). These immunofluorescent stains of liver sections also revealed a significant difference in the lymphoid organization of IgM$^+$ and IgG$^+$ B cells in the liver. Liver sections from HBVEnv*Rag1*$^{-/-}$ mice acquired 21 days after adoptive transfer of WT splenocytes revealed that IgG$^+$ B cells clustered in the liver parenchyma and coclustered with IgM$^+$ B cells (Figure 6, B and D). Furthermore, these IgG$^+$ clusters colocalized to the macrophage clusters (Figure 6E). In contrast, liver sections acquired from HBVEnv*Rag1*$^{-/-}$ mice 21 days after adoptive transfer of *Cxcr5*$^{-/-}$ splenocytes revealed significantly fewer IgG$^+$ B cell clusters and significantly fewer IgG$^+$ and IgM$^+$ B cell coclusters (Figure 6, B and D).

CXCL13 is expressed in an age-dependent manner in human liver and is increased in the plasma of patients who clear HBV. Because of the essential role played by CXCR5 and CXCL13 in the development of an effective HBV immune response in our mouse model, we hypothesized that the age-dependent expression of CXCL13 observed in mouse liver might also hold true for humans. To address this question, we obtained paraffin-embedded human liver biopsy tis-

sue from infant (6–12 weeks of age) and adult livers. Analysis of relative expression of *CXCL13* mRNA derived from these samples revealed clear evidence that *CXCL13* was also expressed in an age-dependent manner in human liver (Figure 7A).

To further validate a role for CXCR5 and CXCL13 in facilitating human HBV clearance, we studied plasma from patients infected with HBV to identify an association between plasma CXCL13 levels and an effective immune response in humans clearing a-HBV. We were encouraged to use this approach because studies in the mouse model demonstrated that plasma expression of CXCL13 reflected levels in the liver (Supplemental Figure 7). We found that adult patients with acute hepatitis B had increased plasma CXCL13 levels during the primary immune response to HBV that resulted in viral clearance and immunity (Figure 7B). These increased CXCL13 levels did not accompany the futile immune response that occurs during a hepatitic flare in patients chronically infected with HBV (Figure 7B). Thus, increased plasma CXCL13 was distinctly observed in HBV patients who go on to clear the virus, and was not seen in chronically infected patients with similar HBV viral loads and liver inflammation.

Discussion

Our present findings indicated that efficient HBV-specific adaptive immunity is primed in the liver, with CXCL13$^+$ macrophages playing a key role. The concept of immune priming in the liver is controversial, with contradictory results depending on the model or antigen used. In general, hepatic immune priming is considered to favor immune tolerance rather than immune activation (19–22). However, given the prevalence of hepatotropic viral pathogens and the liver's demonstrated ability to naturally protect itself, the organ must possess the capacity to facilitate immune activation and antiviral immunity. The data presented here, and in our earlier experiments (9), collectively identified key age-dependent capabilities in mechanisms of hepatic immune activation.

Several research groups have studied hepatic immune activation using models of liver transplantation, transgenic expression of antigen in the liver, viral-induced liver inflammation, and analysis of hepatic lymphocytic aggregates after immunization at a distant site. These careful studies have demonstrated that CD4$^+$ and CD8$^+$ T cell responses can be primed in the liver (23–28). There was no evidence of B cell priming or differentiation in the liver in any of these models. Taken together, these studies support the hypothesis that immune priming can occur in the liver and that this priming is likely important in pathophysiological conditions in which infection is primarily in the liver.

In addition, research groups have addressed the role of macrophages in controlling viral infection and also in contributing to liver disease pathogenesis. Splenic red pulp macrophages have been found to be necessary for T cell priming to vesicular stomatitis virus (29), and splenic marginal zone macrophages have been shown to contribute to early control of lymphocytic choriomeningitis virus infection (30). However, in these studies, there was no evidence supporting a role for macrophages in lymphoid organization. Furthermore, other research groups have demonstrated various roles for macrophages in liver injury or liver repair. In many models of liver injury, hepatic macrophages themselves are involved in the pathogenesis of the liver damage (31). In other models, macrophages play a role in preventing severe hepatic immunopathology (32) or in limiting the severity of liver immunopathology (33). These particular mechanisms do not appear to play a significant role in our HBV model, as mice lacking macrophages or CXCL13/CXCR5 did not have a significant difference in liver injury, despite developing significantly different immune responses to HBV (Figures 3, 5, and 6).

Here, we demonstrated that the immune response to the hepatotropic pathogen HBV was both primed and centered in the liver. Using a mouse model of primary infection, we showed that T cells specific to multiple HBV epitopes were first detected in the liver 3 days after adoptive transfer of splenocytes, followed by an even more robust response after 8 and 12 days. On day 3 after adoptive transfer, we did not detect HBV-specific T cell responses in the spleen or in LNs at sites entering and draining the liver. On day 8, in addition to the robust HBV-specific T cell response detected in the liver, we began to detect a small HBV-specific response from CD4$^+$ T cells in the HLNs that drain the liver. It was not until 12 days after adoptive transfer that we began to detect a systemic HBV-specific response in the spleen and LNs. Additionally, HBV-specific IL-21 expression, which we have previously shown to be produced principally by TFH and to be crucial in facilitating effective HBV-specific T cell and B cell responses (9), was only detected in the liver, beginning 8 days after adoptive transfer, and was not detected in the spleen or LNs.

Furthermore, we demonstrated that the ability to prime an effective hepatic immune response to HBV was greatly influenced by development of lymphoid organization within the liver, which facilitates the colocalization of antigen-presenting cells with B and T cells. Our data suggest that lymphoid organization in liver is distinct from lymphoid organization in conventional lymphoid organs and that CXCL13-producing liver macrophages are a crucial component, important for the generation of an effective immune response to HBV. We also demonstrated that macrophage-associated lymphoid organization was greatly diminished in young mice that have ineffective immune priming to HBV. A potentially broader role for hepatic macrophages in facilitating lymphoid organization and immune activation in humans is supported by the prior observation that macrophage and T cell clusters form in the livers of patients with chronic hepatitis C (34).

Our data suggest a model in which age-dependent differences in liver macrophages profoundly influence hepatic lymphoid organization and immune priming, and an effective adaptive immune response to HBV. This is supported by our observation that young HBVEnv*Rag1*$^{-/-}$ mice developed minimal macrophage-associated lymphoid organization after adoptive transfer of splenocytes and by our demonstration that selective depletion of hepatic macrophages led to impaired B and CD4$^+$ T cell clustering in the liver and an ineffective immune response to HBV. In addition, the chemokine CXCL13 was expressed in an age-dependent manner predominantly on liver macrophages, and the timing of expression of CXCL13 synchronized with the ability to convert an ineffective immune response to HBV to an effective response. Furthermore, the CXCR5-CXCL13 interaction was necessary for HBsAg clearance, HBsAb production, and HBV-specific T cell diversity, and increased plasma CXCL13 levels were associated with a primary immune response to HBV that resulted in viral clearance and immunity. Taken together, these data strongly suggest that CXCL13 expression on liver macrophages is crucial for effective priming and natural immunity to HBV. Although CXCL13 expression in macrophages has previously been shown to be important in lymphoid neogenesis in mouse and human inflammatory diseases (35–37) and in production

of natural antibodies (38), to our knowledge, a role for macrophage-derived CXCL13 in promoting B and T cell responses to infection has not previously been described.

As with all animal models of human disease, certain aspects of natural HBV infection are not captured. For example, the mice are not naturally infected by HBV, but are producing transgenic HBV proteins and virions. Also, in the HBV transgenic model, a naive immune system abruptly encounters hepatocytes expressing high levels of HBV antigen or virions. Whether kinetic differences in HBV infection and replication also influence the evolution of the immune response, as suggested by a different animal model (39), remains to be determined.

HBV seems to have evolved to exploit a gap in the development of hepatic immune competence by infecting neonates and young children. Why an early gap in hepatic immunity exists is unclear, and it is noteworthy that HBV does not tend to affect gene flow and therefore should not exert host selection pressure that might propel faster constitution of the adult hepatic immune state, even in highly HBV-prevalent populations. However, our present study identified previously unrecognized, and potentially therapeutically relevant, components of hepatic immunity by associating their age-dependent absence and presence with, respectively, persistence and clearance of viral antigenemia.

Finally, the age-dependent expression of CXCL13 in the liver of both mice and humans strongly suggests that the ineffective immune response to HBV observed in young mice and young humans is partially explained by this phenomenon. However, the observation that macrophage-associated lymphoid organization seems largely intact in both adult HBVEnv*Rag1*$^{-/-}$ recipients of *Cxcr5*$^{-/-}$ splenocytes and in HBVEnv*Rag1*$^{-/-}$*Cxcl13*$^{-/-}$ recipients of WT splenocytes, but greatly diminished in young mice, suggests that expression of additional age-dependent molecules on liver macrophages also facilitates lymphoid organization and effective immune priming in the liver. This hypothesis is also supported by our observation that lymphocyte clustering and IL-21 production is greatly diminished in mice depleted of macrophages, but largely intact in both adult HBVEnv*Rag1*$^{-/-}$ recipients of *Cxcr5*$^{-/-}$ splenocytes and in HBVEnv*Rag1*$^{-/-}$*Cxcl13*$^{-/-}$ recipients of WT splenocytes.

Taken together, our prior (9) and present results begin to define some of the immunological mechanisms necessary for effective viral control and some of the potential molecular and cellular pathways to target for potential therapeutic benefit. Our current data suggests that initiation of an effective immune response to HBV occurs in hepatic lymphoid structures that support initiation of primary T cell responses, including classical CD4$^+$ and CD8$^+$ cell priming, as well as priming of TFH cells. In addition, the hepatic lymphoid structures support differentiation and maturation of B cell responses. Notably, a recent publication suggests that signaling via TLR9 might contribute to the development of these hepatic lymphoid structures (40). However, the hepatic lymphoid structures that are a consequence of TLR9 agonists are not composed of the full spectrum of cells we observed in the adult mice in response to HBV, and they do not facilitate initiation of primary T cell responses or contain B cells. Deeper knowledge of the constellation of cells and signals that regulate these processes will facilitate greater mechanistic understanding of the development and regulation of liver immunity and identify new potential therapeutic targets that may lead to treatment strategies for HBV, for other hepatotropic pathogens, and for liver inflammation.

Methods

Mice. WT C57BL/6 mice were purchased from Jackson Laboratory. *Cxcr5*$^{-/-}$ mice were provided by J. Cyster (UCSF, San Francisco, California, USA; ref. 17). HBVtg*Rag1*$^{-/-}$ mice were previously described (11). HBVEnv*Rag1*$^{-/-}$ mice were generated using HBV-Env$^+$ mice (lineage 107-5D; gift from F. Chisari, Scripps Research Institute, La Jolla, California, USA; ref. 41) backcrossed to *Rag1*$^{-/-}$ C57BL/6 mice for 15 generations. HBVEnv*Rag1*$^{-/-}$ mice contain the entire envelope (subtype ayw) protein-coding region under the constitutive transcriptional control of the mouse albumin promoter. HBVEnv*Rag1*$^{-/-}$*Cxcl13*$^{-/-}$ mice were generated by crossing *Cxcl13*$^{-/-}$ C57BL/6 mice (gift from J. Cyster; ref. 42) to HBVEnv*Rag1*$^{-/-}$ mice.

Young (3–4 weeks old, preweaned) or adult (8–12 weeks old) HBVtg*Rag1*$^{-/-}$ mice were given 10^8 syngeneic splenocytes from WT or mutant mouse strains via tail vein injection. Young mice were weaned at date of transfer. Clodronate-treated mice received clodronate liposomes on days –1, 2, and 5 relative to adoptive transfer (designated day 0) for day-8 experiments, or on days –1, 2, 5, 8, and 11 for long-term experiments. Cl_2MDP (clodronate) was a gift of Roche Diagnostics GmbH. Clodronate liposomes were prepared as described previously (13).

Mice were followed for alanine aminotransferase using an ALT-L3K kit (Diagnostic Chemicals Ltd.) on a Cobas Miras Plus analyzer (Roche Diagnostics). Mice were kept in microisolater cages in a specific pathogen–free facility.

HBV protein assays. Plasma was collected and assayed for the presence of HBsAg by using ETI-MAK 2Plus (DiaSorin). HBsAb results are reported as positive or negative, determined by parameters programed in Diasorin plate reader. HBsAb was quantified by using ETI-AB-AUK-PLUS and ABAU standard set (Diasorin). This kit detects all isotypes of HBsAb and has a sensitivity of 5 MIU/ml. Plasma from transferred HBVRplRag mice was assayed for presence of HBcAb using ETI-AB-COREK-PLUS (Diasorin). All assays were read on ELx800 (Biotek Instruments Inc.) at a wavelength of 450 nm and 630 nm.

Cell preparations. Liver lymphocytes were isolated from the liver after perfusion and digestion. Briefly, mice were perfused via the inferior vena cava using digestion media (RPMI-1640 containing 5% FBS; 0.2 mg/ml crude collagenase, Crescent Chemical; and 0.02 mg/ml DNase I, Roche Diagnostics). Livers were forced through a 70-μM filter using a syringe plunger, and debris was removed by centrifugation (30 *g* for 3 minutes). Supernatants were collected and centrifuged for 10 minutes at 650 *g*. Lymphocytes were isolated using a 60:40 Percoll gradient. Lymphocytes from spleen and LNs were isolated using standard methods.

Macrophage fractions were isolated from the liver after 3 minutes of perfusion via the inferior vena cava using digestion media as above. Livers were chopped with scissors and incubated at 37°C in a shaking water bath in pronase digestion media (RPMI-1640 containing 5% FBS; 0.44 mg/ml pronase, Roche Diagnostics; and 0.008 mg/ml DNase I, Roche Diagnostics). Livers were gently passed through a 70-μM filter, and debris was removed by centrifugation (30 *g* for 3 minutes). Supernatants were collected and centrifuged for 10 minutes at 650 *g*. Lymphocytes were isolated using a 25:50 Percoll gradient. Hepatocytes were isolated from *Rag1*$^{-/-}$ mouse livers by collagenase perfusion followed by density gradient centrifugation. Viability of hepatocytes was ≥95%.

T and B cell assays. Peptide pool ELISpot assays were performed using IFN ELISpot (BD Biosciences) assays plated with lymphocytes from liver, spleen, and LNs isolated from transferred animals as above, and combined 1:1 with *Rag1*$^{-/-}$ splenocytes to provide optimal antigen-presenting cell stimulation. 15-mer peptides were generated across the whole envelope protein in 11-aa overlaps (Sigma-Aldrich). Pools included 11–14 peptides (9). Cells were incubated with peptides at a final concentration of 5 μg/ml per peptide.

Liver lymphocytes were prepared as described above. Cells were stained according to standard protocols with combinations of the following anti-mouse antibodies (all from eBioscience): allophycocyanin-conjugated or

biotinylated anti–TCR-β (clone H57-597), PerCPCy5.5-conjugated anti-B220 (clone RA3-6B2), Pacific Blue–conjugated anti-CD19 (clone 57-0193), efluor450-conjugated anti-CD44 (clone IM7). After surface staining, cells were fixed and permeabilized using Cytofix/Perm (BD Biosciences) and stained with PE-conjugated anti-CD138 (clone 281-2; BD Biosciences) for 40 minutes at 4°C. Cells were washed and stained overnight at 4°C with PECy7-conjugated anti-IgM (clone 11/14; eBioscience) along with FITC-conjugated anti-IgG1 (clone SB77e; Southern Biotech), FITC-conjugated anti-IgG2b (clone R12-3; BD Biosciences), or FITC-conjugated anti-IgG3 (clone R40-82; BD Biosciences) or appropriate isotype-matched control Ig. Cells were analyzed using an LSRII flow cytometer (BD) and FlowJo software (Tree Star). IFN-γ capture assay was performed according to the manufacturer's instructions (Miltenyi Biotec) with a 4-hour incubation time with HBV peptide pools as described above and previously (9). Following the IFN-γ capture protocol, cells were stained for TCR-β, CD4, and CD8 and analyzed as described above.

Isolation of liver cell populations. Liver lymphocytes were isolated and stained as described above. Single cells were sorted using FACS Aria (BD Biosciences) for viability and the following markers for the given populations: $NK1.1^+$ for NK cells; $NK1.1^-CD11c^+CD11b^-$ for DCs; $NK1.1^-CD11b^+F4/80^-$ for granulocytes/monocytes. Macrophages were isolated from the macrophage-enriched protocol and stained as described above. Single cells were sorted for viability and $CD45^+F4/80^+CD11b^+$. Hepatocytes were isolated as described above and sorted for viability and size. All populations were confirmed by flow cytometry prior to RNA isolation. RNA was isolated using RNeasy micro kit and amplified for CXCL13 as described below.

Liver immunofluorescent stain. Liver tissue was collected and flash frozen in OCT using liquid nitrogen bath. Frozen tissue was cut at 0.6 μm and fixed in acetone for 10 minutes. Tissue was stained using Perkin Elmer TSA signal amplification kit. Briefly, slides were thawed and rehydrated in a PBS bath and incubated for 1 hour in 1% H_2O_2 and 0.1% sodium azide on a shaker at room temperature. Slides were washed and blocked with Fc Block (BD Bioscience) and 1% rat serum (eBioscience) for 1 hour at room temperature (RT) in a humidifying rack. Slides were washed and incubated at RT with streptavidin block for 20 minutes, followed by biotin block for 20 minutes (Streptavidin/Biotin Block; Vector Labs). Slides were incubated overnight at 4°C with primary antibody. Slides were washed and stained for 30 minutes at RT with streptavidin-HRP, followed by a wash and 7-minute incubation at RT with Alexa Fluor 555–tyramide. Slides were incubated in 1% H_2O_2 and 0.1% sodium azide, streptavidin, and biotin as described above, followed by 1-hour incubation with primary antibody at RT. Slides were washed and stained for 30 minutes at RT with streptavidin-HRP, followed by a wash and 6-minute incubation at RT with FITC-tyramide. Slides were washed, stained with DAPI for 5 minutes, and mounted. Fluorescent tissue was visualized and photographs captured on AxioVision software and Axio Imager M2 Upright Microscope (Zeiss). Antibodies used were as follows: CD4-biotin (clone RM4-5; BD Bioscience), B220-biotin (RA3-6B2; BD Biosciences), CD8-biotin (clone KT15; AbD serotec), F4/80-biotin (clone BM8; eBioscience), IgG (IgG1-biotin [clone A85-1; BD Bioscience] plus IgG2b-biotin [clone RMG2b-1; Biolegend]), IgM-biotin (clone RMM-1; Biolegend), CD11c-biotin (clone HL3; BD Bioscience).

RNA extraction and real-time PCR. RNA isolated from lymphocytes and LNs was prepared using an RNeasy micro kit (Qiagen) with a blunt syringe and QIAshredder (Qiagen) disruption. RNA isolated from liver and spleen tissue was prepared using RNeasy mini kit (Qiagen) using bead beat lysing (MP Biomedicals) and Qiashredder (Qiagen) disruption. 1 or 0.25 μg isolated RNA was reverse transcribed using iScript cDNA synthesis kit (BioRad). Real-time PCR was performed on 2.5 μl cDNA product using iTaq SYBR Green Supermix with ROX (BioRad) and the following primers: *Gapdh* forward, 5′-GGAGCGAGACCCCACTAACA-3′; *Gapdh* reverse, 5′-ACATACTCAGCACCGGCCTC-3′; *Il21* forward, 5′-TCATCATTGACCTCGTGGCCC-3′; *Il21* reverse, 5′-ATCGTACTTCTCCACTTGCAATCC-3′; *Cxcl13* forward, 5′-TGGCCAGCTGCCTCTCTC-3′; *Cxcl13* reverse, 5′-TGGAAATCACTCCAGAACACCTAC-3′. Real-time PCR was performed on 7300 Real Time PCR System (Applied Biosystems).

Patient samples and CXCL13 RNA expression. 24 infants (6–12 weeks of age) were liver biopsied to rule out biliary atresia at UCSF Medical Center (San Francisco, California, USA). Of these patients, 6 were found to have biliary atresia, 6 had neonatal nonviral hepatitis, 10 had a nonspecific liver disease diagnosis including cholestatsis and ductopenia, and 2 had an unknown diagnosis. 9 adult liver biopsies were obtained from donor liver prior to transplantation at California Pacific Medical Center (San Francisco, California, USA). RNA from formalin-fixed, paraffin-embedded tissue was extracted using RNeasy FFPE kit (Qiagen). 150 ng isolated RNA was reverse transcribed using Quantifast Probe assay (Qiagen) and amplified using specific probes and primers to human *GAPDH* and *CXCL13* (proprietary; Qiagen). Plasma was obtained from 5 patients with confirmed a-HBV infection at the time of active hepatitis and confirmed subsequent viral clearance and HBsAb seroconversion, 5 patients with confirmed chronic HBV infection exhibiting a flare of disease, and 6 healthy volunteers and assayed for CXCL13 levels by ELISA (R&D Systems). Blood samples were drawn by a licensed phlebotomist alongside clinical serology samples. Serology, serum HBV DNA, and ALT data were obtained from the patients' clinical medical records with permission. Acutely infected HBV patients had confirmed high viral loads ($2.442 \times 10^7 \pm 2.439 \times 10^7$), elevated ALT (922–2,400 U/l), $HBsAg^+$ and IgM core antibody–positive, and a clinical history of exposure. Chronic HBV patients exhibiting a flare in disease had confirmed high viral loads ($3.058 \times 10^8 \pm 3.047 \times 10^8$), elevated ALT (92–1,090 U/l), $HBsAg^+$, and known history of chronic infection. Uninfected controls had confirmed low ALT (16–32 U/l) and were $HBsAg^-$.

Statistics. Statistics were performed using Prism (Graph Pad Software). Statistical significance was determined by 2-tailed unpaired Student's *t* test (when 2 groups were compared), Mann-Whitney test (for patient studies), or Tukey's ANOVA multiple-comparison test (when more than 1 group was compared). For significance of HBsAg clearance, in which 1 of 2 possible outcomes was compared (clearance versus no clearance), Fisher's χ^2 test was used. In all figures with multiple *n*, data are presented as mean ± SEM. A *P* value less than 0.05 was considered significant.

Study approval. UCSF Institutional Animal Care and Use Committee approved all animal experiments done in this study. California Pacific Medical Center Institutional Review Board and UCSF Institutional Review Board approved all human studies. Subjects provided informed consent prior to their participation in the study.

Acknowledgments

The authors thank Jay Ryan for advice and critical comments on the manuscript and Anna Bogdanov, Kahee Jo, Richard Locksley, Adam Savage, Mehrdad Matloubian, Mark Ansel, Caroline Miller, Kate Bummer, Sandra Huling, Courtney Crane, Lia Avanesyan and UCSF SABRE Center Functional Genomics Core (Andrea Barczak and Rebecca Barbeau), and Aracely Tamayo for technical assistance and advice. This work was supported by NIAID and NIDDKK (grants R01AI068090, R56AI091872, and R01DK093646-02), UCSF Liver Center (grant P30DK026743), Burroughs Wellcome Fund, and Ibrahim El-Hefni Technical Training Foundation. Throughout the present study, J. Publicover was supported by the A.P. Gianinni Foundation.

Received for publication December 11, 2012, and accepted in revised form June 6, 2013.

Address correspondence to: Jody Baron, 513 Parnassus Ave., Box 0538, Room S 357C, San Francisco, California 94143, USA. Phone: 415.476.5728; Fax: 415.476.0659; E-mail: Jody.baron@ucsf.edu.

R. Lee Reinhardt's present address is: Department of Immunology, Duke University Medical Center, Durham, North Carolina, USA.

Christine Van Horn's present address is: Department of Pathology and Laboratory Medicine, University of California, Los Angeles, California, USA.

1. Lee WM. Hepatitis B virus infection. *N Engl J Med*. 1997;337(24):1733–1745.
2. Robinson WS. *Principles and Practice of Infectious Diseases*. 4th ed. London, United Kingdom: Churchill Livingstone; 1995.
3. Ganem D, Prince AM. Hepatitis B virus infection--natural history and clinical consequences. *N Engl J Med*. 2004;350(11):1118–1129.
4. Liang TJ. Hepatitis B: the virus and disease. *Hepatology*. 2009;49(5 suppl):S13–S21.
5. Nebbia G, Peppa D, Maini MK. Hepatitis B infection: current concepts and future challenges. *QJM*. 2012;105(2):109–113.
6. Bertoletti A, Ferrari C. Innate and adaptive immune responses in chronic hepatitis B virus infections: towards restoration of immune control of viral infection. *Gut*. 2012;61(12):1754–1764.
7. Dandri M, Locarnini S. New insight in the pathobiology of hepatitis B virus infection. *Gut*. 2012; 61(suppl 1):i6–i17.
8. Chisari FV, Isogawa M, Wieland SF. Pathogenesis of hepatitis B virus infection. *Pathol Biol (Paris)*. 2010; 58(4):258–266.
9. Publicover J, et al. Interleukin-21 is pivotal in determining age-dependent effectiveness of immune responses in a mouse model of human hepatitis B. *J Clin Invest*. 2011;121(3):1154–1162.
10. Mombaerts P, Iacomini J, Johnson RS, Herrup K, Tonegawa S, Papaioannou VE. RAG-1-deficient mice have no mature B and T lymphocytes. *Cell*. 1992;68(5):869–877.
11. Baron JL, Gardiner L, Nishimura S, Shinkai K, Locksley R, Ganem D. Activation of a nonclassical NKT cell subset in a transgenic mouse model of hepatitis B virus infection. *Immunity*. 2002; 16(4):583–594.
12. Hultkrantz S, Ostman S, Telemo E. Induction of antigen-specific regulatory T cells in the liver-draining celiac lymph node following oral antigen administration. *Immunology*. 2005;116(3):362–372.
13. Van Rooijen N, Sanders A. Kupffer cell depletion by liposome-delivered drugs: comparative activity of intracellular clodronate, propamidine, and ethylenediaminetetraacetic acid. *Hepatology*. 1996; 23(5):1239–1243.
14. Hardtke S, Ohl L, Forster R. Balanced expression of CXCR5 and CCR7 on follicular T helper cells determines their transient positioning to lymph node follicles and is essential for efficient B-cell help. *Blood*. 2005;106(6):1924–1931.
15. Muller G, Hopken UE, Lipp M. The impact of CCR7 and CXCR5 on lymphoid organ development and systemic immunity. *Immunol Rev*. 2003; 195:117–135.
16. Junt T, et al. CXCR5-dependent seeding of follicular niches by B and Th cells augments antiviral B cell responses. *J Immunol*. 2005;175(11):7109–7116.
17. Forster R, Mattis AE, Kremmer E, Wolf E, Brem G, Lipp M. A putative chemokine receptor, BLR1, directs B cell migration to defined lymphoid organs and specific anatomic compartments of the spleen. *Cell*. 1996;87(6):1037–1047.
18. Voigt I, Camacho SA, de Boer BA, Lipp M, Forster R, Berek C. CXCR5-deficient mice develop functional germinal centers in the splenic T cell zone. *Eur J Immunol*. 2000;30(2):560–567.
19. Calne RY. Immunological tolerance — the liver effect. *Immunol Rev*. 2000;174:280–282.
20. Knolle PA, Gerken G. Local control of the immune response in the liver. *Immunol Rev*. 2000;174:21–34.
21. Sato K, Yabuki K, Haba T, Maekawa T. Role of Kupffer cells in the induction of tolerance after liver transplantation. *J Surg Res*. 1996;63(2):433–438.
22. Crispe IN. Liver antigen-presenting cells. *J Hepatol*. 2011;54(2):357–365.
23. Crispe IN. The liver as a lymphoid organ. *Annu Rev Immunol*. 2009;27:147–163.
24. Thomson AW, Knolle PA. Antigen-presenting cell function in the tolerogenic liver environment. *Nat Rev Immunol*. 2010;10(11):753–766.
25. Wuensch SA, Pierce RH, Crispe IN. Local intrahepatic CD8+ T cell activation by a non-self-antigen results in full functional differentiation. *J Immunol*. 2006;177(3):1689–1697.
26. Greter M, Hofmann J, Becher B. Neo-lymphoid aggregates in the adult liver can initiate potent cell-mediated immunity. *PLoS Biol*. 2009;7(5):e1000109.
27. Klein I, Crispe IN. Complete differentiation of CD8+ T cells activated locally within the transplanted liver. *J Exp Med*. 2006;203(2):437–447.
28. Derkow K, et al. Differential priming of CD8 and CD4 T-cells in animal models of autoimmune hepatitis and cholangitis. *Hepatology*. 2007; 46(4):1155–1165.
29. Ciavarra RP, Buhrer K, Van Rooijen N, Tedeschi B. T cell priming against vesicular stomatitis virus analyzed in situ: red pulp macrophages, but neither marginal metallophilic nor marginal zone macrophages, are required for priming CD4+ and CD8+ T cells. *J Immunol*. 1997;158(4):1749–1755.
30. Seiler P, Aichele P, Odermatt B, Hengartner H, Zinkernagel RM, Schwendener RA. Crucial role of marginal zone macrophages and marginal zone metallophils in the clearance of lymphocytic choriomeningitis virus infection. *Eur J Immunol*. 1997; 27(10):2626–2633.
31. Kolios G, Valatas V, Kouroumalis E. Role of Kupffer cells in the pathogenesis of liver disease. *World J Gastroenterol*. 2006;12(46):7413–7420.
32. Lang PA, et al. Tissue macrophages suppress viral replication and prevent severe immunopathology in an interferon-I-dependent manner in mice. *Hepatology*. 2010;52(1):25–32.
33. Sitia G, et al. Kupffer cells hasten resolution of liver immunopathology in mouse models of viral hepatitis. *PLoS Pathog*. 2011;7(6):e1002061.
34. Burgio VL, Ballardini G, Artini M, Caratozzolo M, Bianchi FB, Levrero M. Expression of co-stimulatory molecules by Kupffer cells in chronic hepatitis of hepatitis C virus etiology. *Hepatology*. 1998; 27(6):1600–1606.
35. Carlsen HS, Baekkevold ES, Morton HC, Haraldsen G, Brandtzaeg P. Monocyte-like and mature macrophages produce CXCL13 (B cell-attracting chemokine 1) in inflammatory lesions with lymphoid neogenesis. *Blood*. 2004;104(10):3021–3027.
36. Moreth K, et al. The proteoglycan biglycan regulates expression of the B cell chemoattractant CXCL13 and aggravates murine lupus nephritis. *J Clin Invest*. 2010;120(12):4251–4272.
37. Schiffer L, et al. Activated renal macrophages are markers of disease onset and disease remission in lupus nephritis. *J Immunol*. 2008;180(3):1938–1947.
38. Ansel KM, Harris RB, Cyster JG. CXCL13 is required for B1 cell homing, natural antibody production, and body cavity immunity. *Immunity*. 2002;16(1):67–76.
39. Wieland S, Thimme R, Purcell RH, Chisari FV. Genomic analysis of the host response to hepatitis B virus infection. *Proc Natl Acad Sci U S A*. 2004; 101(17):6669–6674.
40. Huang LR, et al. Intrahepatic myeloid-cell aggregates enable local proliferation of CD8(+) T cells and successful immunotherapy against chronic viral liver infection. *Nat Immunol*. 2013; 14(6):574–583.
41. Chisari FV, et al. Expression of hepatitis B virus large envelope polypeptide inhibits hepatitis B surface antigen secretion in transgenic mice. *J Virol*. 1986; 60(3):880–887.
42. Ansel KM, et al. A chemokine-driven positive feedback loop organizes lymphoid follicles. *Nature*. 2000; 406(6793):309–314.